Supplement of Clim. Past, 22, 989–1002, 2026
https://doi.org/10.5194/cp-22-989-2026-supplement

Climate of the Past Open Access EGU

Supplement of

Limited early-industrial warming and strong volcanic imprints in the Caucasus: the first temperature reconstruction based on maximum latewood density

Rupesh Dhyani et al.

Correspondence to: Rupesh Dhyani (rupesh.dhyani@geogr.uni-giessen.de)

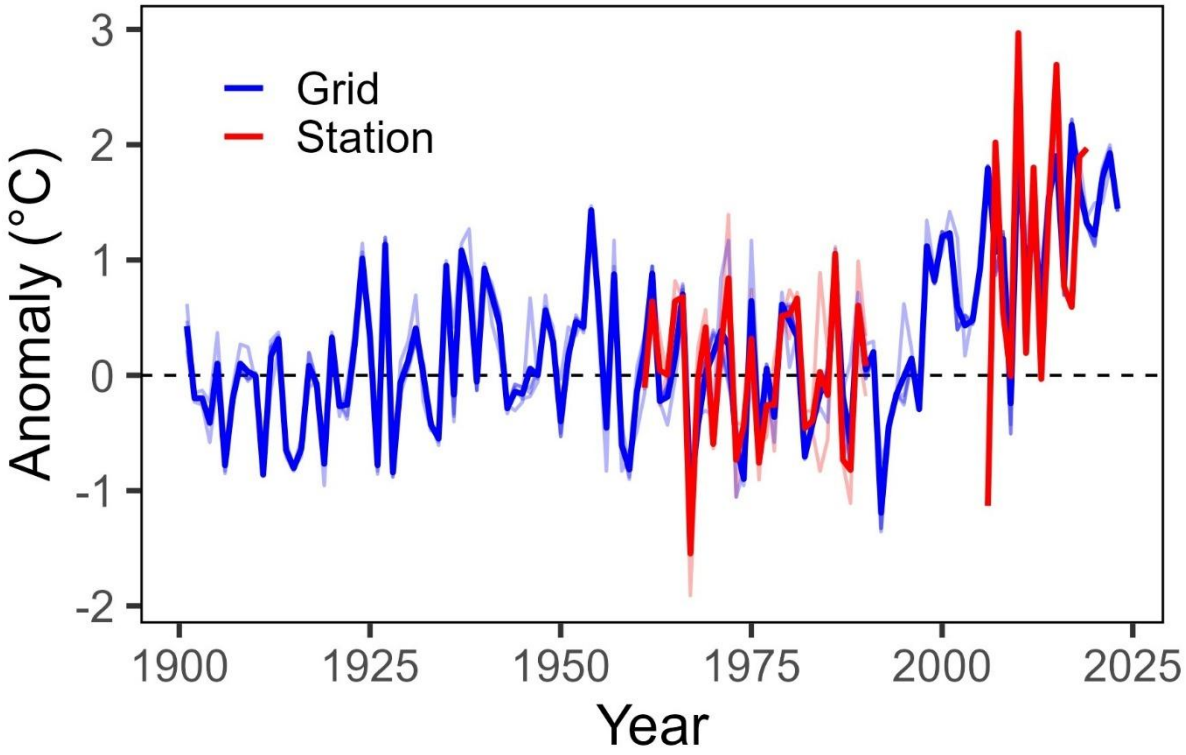

Figure S1: Standardized June–August (JJAS) temperature anomalies. The mean of two station records, Ardahan (41.10N, 42.70E, 1829.0m) and Artvin (41.17N, 41.82E, 30.0m), is compared to the mean of three closest CRU TS 4.09 temperature series (Grid 1: 41.75° N, 42.75° E; Grid 2: 41.25° N, 42.25° E; Grid 3: 41.25° N, 42.75° E). Shaded lines represent the individual timeseries. Anomalies were calculated with respect to the reference period 1961-1990.

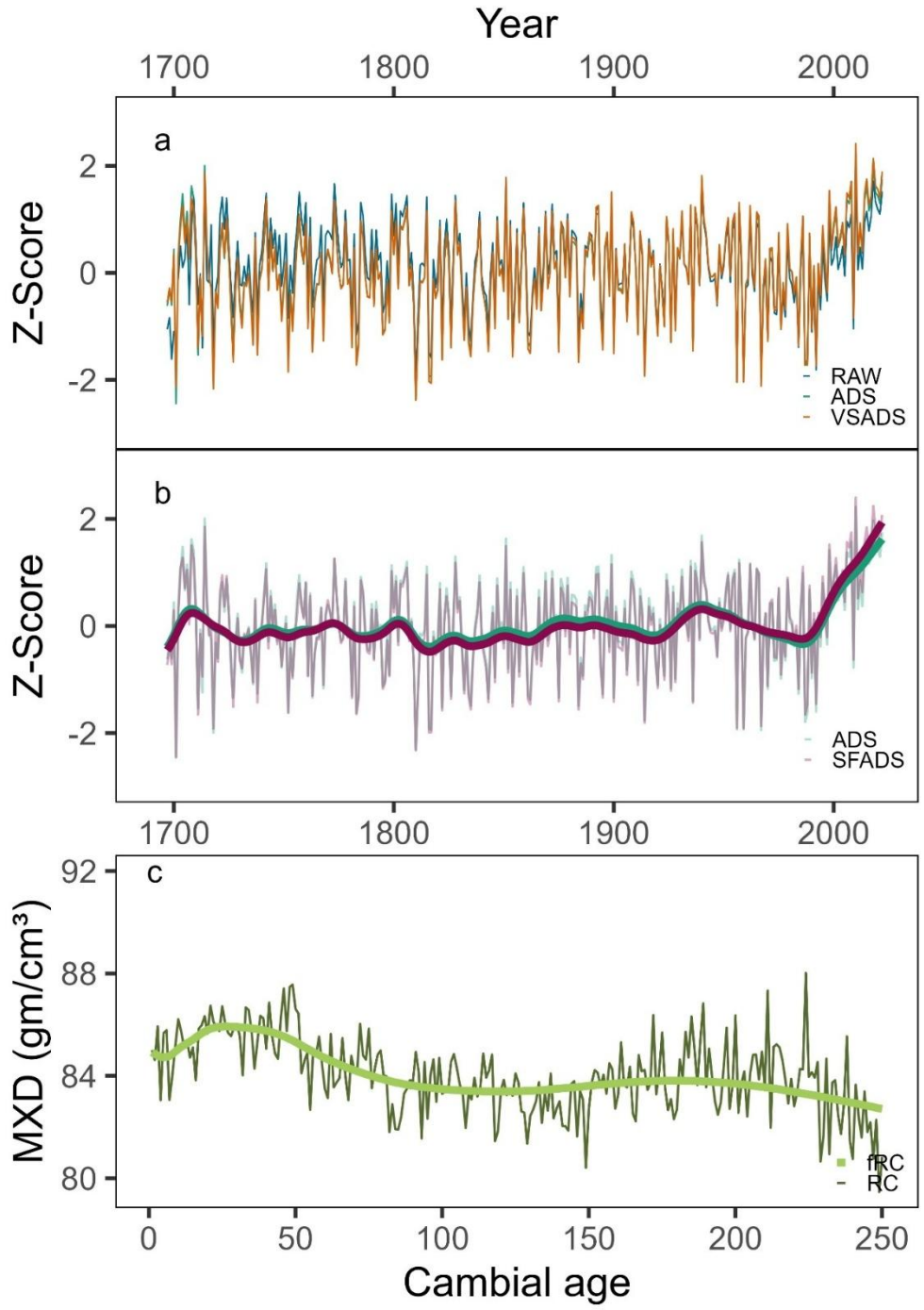

Figure S2: The impact of detrending and standardization methods on the shape of the MXD chronology. Tree-ring MXD chronologies (1697-2022) detrended using different variants of the age dependent spline: (a) comparison between the raw MXD

chronology vs a chronology with age dependent spline detrending (ADS) without and with variance stabilization (VSADS) (b) ADS vs Signal free Age dependent spline detrending (SFADS) with 30-year smoothing splines and (c) the age-aligned Regional Curve displayed for the well-replicated interval with a 30-year smoothing spline.

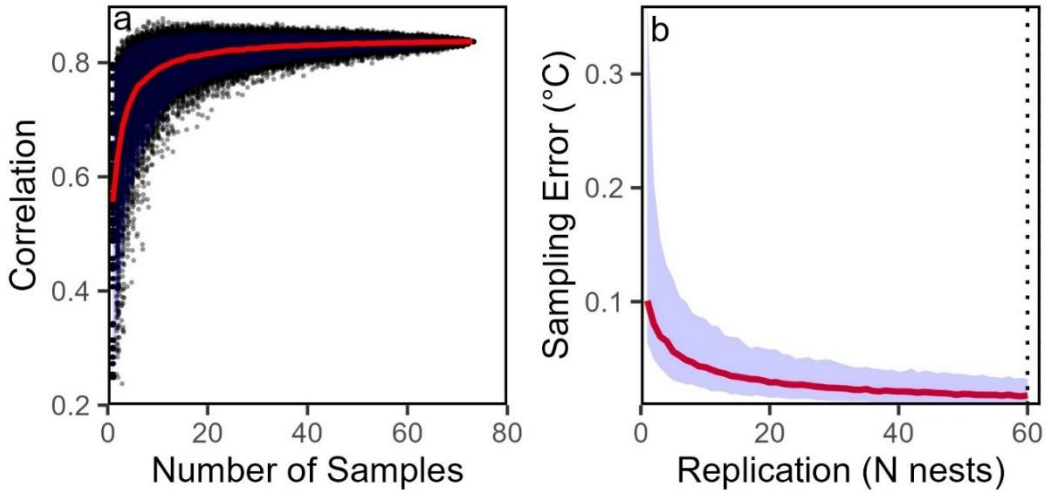

Figure S3: (a) Bootstrapped correlation between the MXD data and JJAS temperature as a function of the number of randomly sampled MXD series (replication size). Each black point represents one of 1,000 iterations per replication level. The red line shows the mean correlation, while the shaded blue area indicates the 95% confidence interval based on the percentile bootstrap and (b) Monte-Carlo estimate of reconstruction sampling error (°C) versus replication (number of nests, *N*). The blue ribbon shows the 5–95% interval and the red line the median. Dotted vertical lines mark the maximum replication actually attained in the dataset.

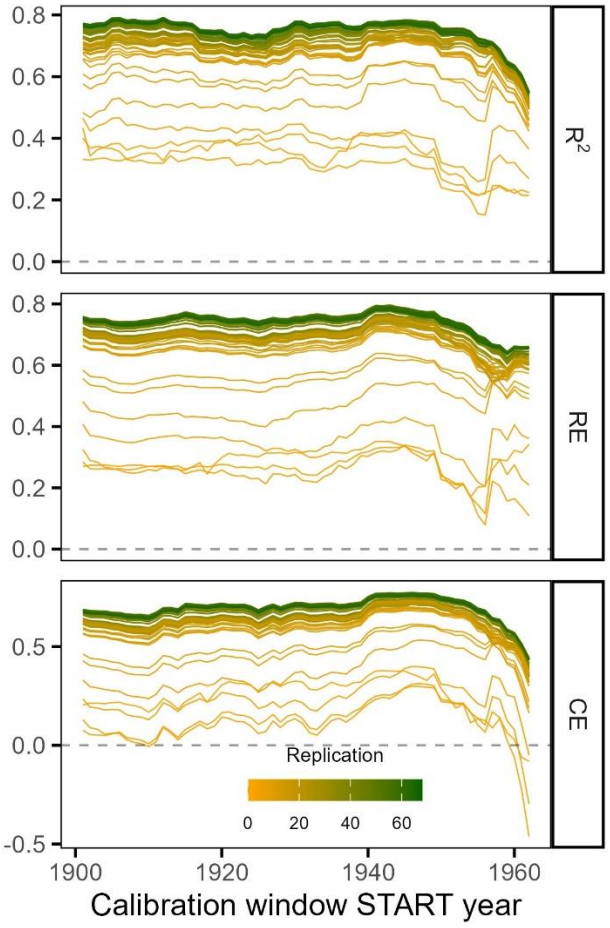

Figure S4: Validation statistics for reconstruction skill. Validation coefficient of determination (R^2), Reduction of Error (RE) and Coefficient of Efficiency across different calibration start years. Note that the validation period starts 61 years before or after the calibration, i.e., if calibration is performed from 1901-1961, validation covers 1962-2022. Each line represents an individual nest, with colour shading indicating replication.

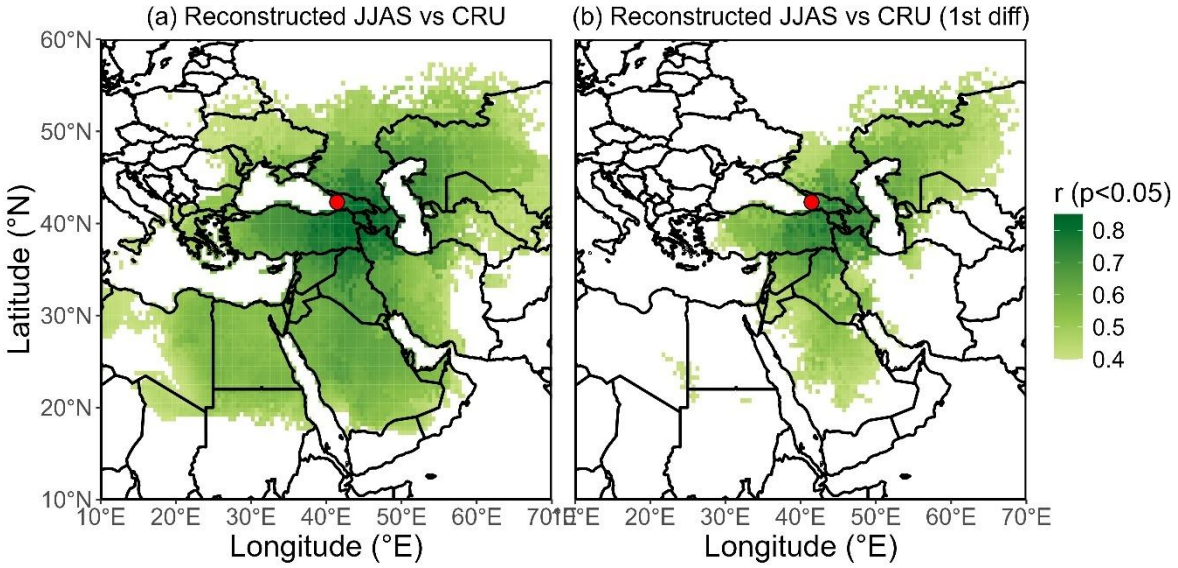

Figure S5: Spatial correlations between the reconstructed JJAS temperature series and JJAS CRU temperature data, using (a) raw data and (b) high-pass filtered data for the period 1901-2022. Only significant correlations are shown in the maps. The site location is marked by red circle.

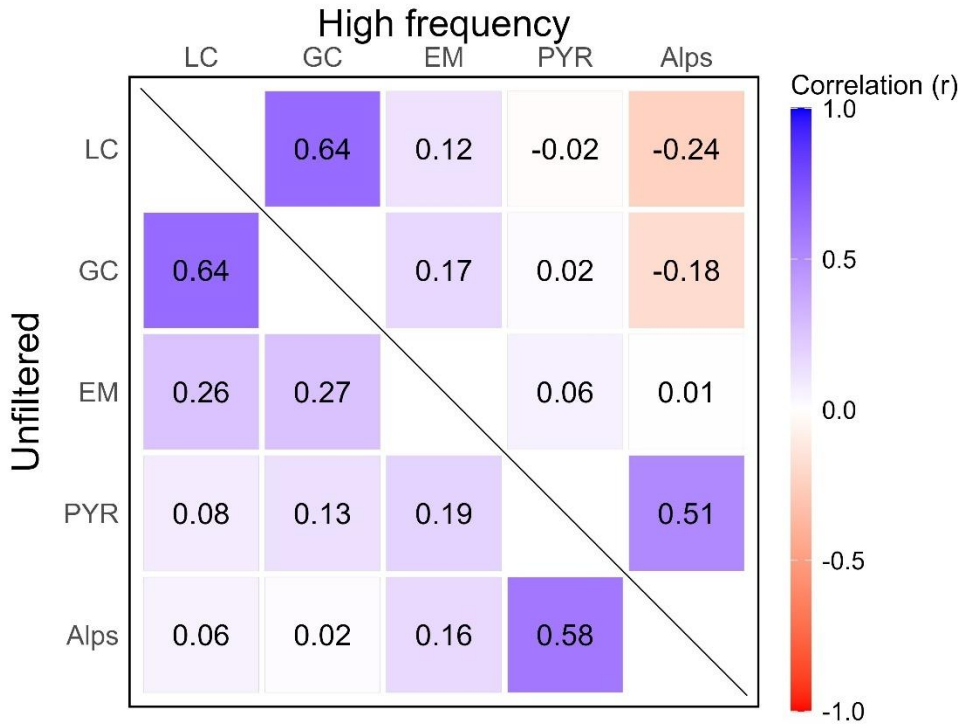

Figure S6: Pearson correlations (r) between the LC reconstruction and other records over their overlapping period (1697 to most recent year). The heatmap shows unfiltered correlations (lower triangle) and correlations after first differencing (upper triangle).

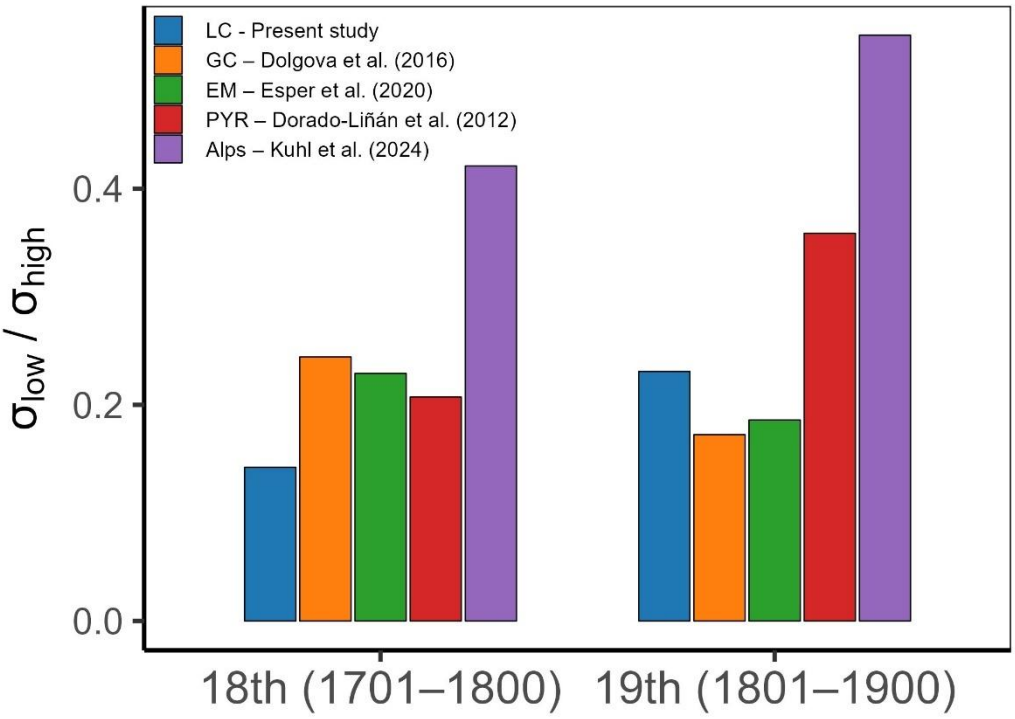

Figure S7: Ratios of standard deviations of low- and high-pass filtered timeseries (30-year moving average) during the 18th and 19th century. Colours are consistent across panels for the LC reconstruction (this study), the Greater Caucasus (Dolgova et al., 2016), the Eastern Mediterranean (Esper et al., 2020), the Pyrenees (Dorado Liñán et al., 2012) and the Alps (Kühl et al., 2024).

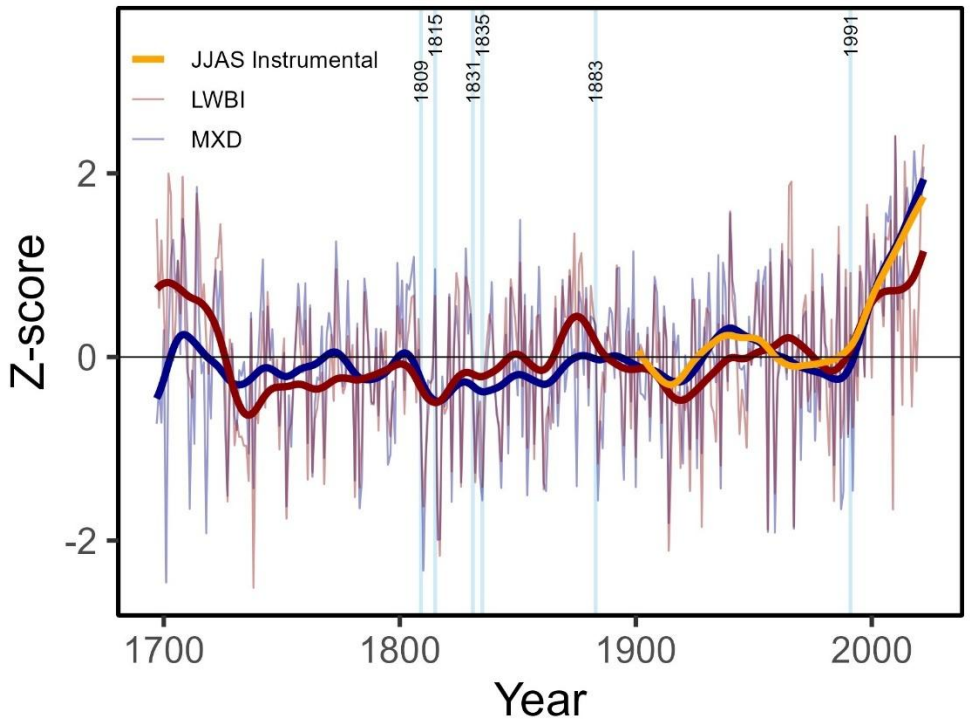

Figure S8: Standardized maximum latewood density (MXD) and latewood blue intensity (LWBI) series from 1697-2022 along with low-pass filtered instrumental JJAS temperature (anomalies w.r.t 1961-1990). Both MXD and LWBI series are detrended using the signal free age dependent spline method and smoothed by 30-year cubic spline used to highlight lower-frequency variability. The light blue vertical lines are labelled with volcanic events. The LWBI data is updated from Dhyani et al. (2025).

Table S1 Metadata for the regional tree-ring proxies datasets used for the comparison in this study. Target seasons refer to the months used for calibration in the original study: M = May, J = June, J = July, A = August, S = September. Correlation values (r) indicate the strength of the relationship with instrumental temperature reported in the original study.

Data	Proxy type	Coordinates	Target season	Correlation (r)	Period used	Reference
Greater Caucasus	LWBI	43.3 N, 42.6 E	JJAS	0.74	1697-2011	(Dolgova, 2016)
Eastern Mediterranean	MXD	40.1 N, 29 E	JAS	0.73	1697-2015	(Esper et al., 2020)
Pyrenees	MXD	42-43 N, 0-1 E	MJJAS	0.62	1697-2005	(Dorado Liñán et al., 2012)
Alps	MXD	-	MJJA	0.80	1697-2017	(Kuhl et al., 2024)

References

Dolgova, E.: June–September temperature reconstruction in the Northern Caucasus based on blue intensity data, Dendrochronologia, 39, 17–23, https://doi.org/10.1016/j.dendro.2016.03.002, 2016.

Dorado Liñán, I., Büntgen, U., González-Rouco, F., Zorita, E., Montávez, J. P., Gómez-Navarro, J. J., Brunet, M., Heinrich, I., Helle, G., and Gutiérrez, E.: Estimating 750 years of temperature variations and uncertainties in the Pyrenees by tree-ring reconstructions and climate simulations, Climate of the Past, 8, 919–933, https://doi.org/10.5194/cp-8-919-2012, 2012.

Esper, J., Klippel, L., Krusic, P. J., Konter, O., Raible, C. C., Xoplaki, E., Luterbacher, J., and Büntgen, U.: Eastern Mediterranean summer temperatures since 730 CE from Mt. Smolikas tree-ring densities, Clim Dyn, 54, 1367–1382, https://doi.org/10.1007/s00382-019-05063-x, 2020.

Kuhl, E., Esper, J., Schneider, L., Trouet, V., Kunz, M., Klippel, L., Büntgen, U., and Hartl, C.: Revising Alpine summer temperatures since 881 CE, Clim Dyn, https://doi.org/10.1007/s00382-024-07195-1, 2024.